From: FRACTURE MECHANICS OF CERAMICS, Vol. 8
Edited by R.C. Bradt, A.G. Evans,
D.P.H. Hasselman, and F.F. Lange
(Plenum Publishing Corporation, 1986)

MICROSTRUCTURE AND THE STRENGTH OF CERAMICS

C.J. Fairbanks, B.R. Lawn, R.F. Cook, and Y.W. Mai*

Center for Materials Science
National Bureau of Standards
Gaithersburg, MD 20899

ABSTRACT

Microstructural influences on ceramic strength become significant at small flaw sizes. These influences are readily quantified by strength testing with controlled indentation flaws. Data are presented here for alumina and glass-ceramic specimens broken under both inert and fatigue conditions. As the flaw size is systematically reduced there is a tendency to a reduction in strength relative to that predicted from macroscopic toughness measurements, reflecting R-curve behavior. This tendency is critically dependent on the microstructural detail, e.g. presence of glassy phases at the grain boundaries in the aluminas. However, the fatigue susceptibility is found to be relatively insensitive to the microstructural influence over the same flaw-size range.

A fracture mechanics framework for incorporating a "microstructural stress intensity factor" is outlined. The description establishes a proper basis for extrapolating fracture data from traditional large-scale crack specimens into the domain of naturally occurring flaws. Direct observations of the indentation crack response during actual strength testing indicates that the principal mechanism of the microstructural "toughening" effect is crack restraint by grain-localized ligamentary "bridging" behind the advancing front.

1. INTRODUCTION

It is now well known that the fracture properties of brittle ceramics can be strongly influenced by the material microstructure.[1] It becomes pertinent to ask whether toughness and crack velocity data on well-developed, macroscopic fracture specimens can be extrapolated to the domain of strength-controlling microscopic flaws. At issue is the long-standing Griffith strength formalism on which all modern-day fracture mechanics design is based.

---

*On leave from the Department of Mechanical Engineering, University of Sydney, N.S.W. 2006, Australia

In confronting this issue we are led to the phenomenon of crack-resistance, or R-curve, behavior. At very small crack sizes relative to the scale of the microstructure the toughness is expected to be determined simply by a bulk cleavage or grain boundary interface energy, depending on whether the fracture mode is transgranular or intergranular. At large crack sizes the toughness can be considerably greater than these intrinsic levels, representative of the polycrystalline aggregate. Hence the toughness is no longer a constant material parameter, but becomes some function of crack size - the R-curve. How, then, may we determine such toughness characteristics experimentally, and thence incorporate these characteristics into a formal fracture mechanics description of strength? What effect does R-curve behavior have on fatigue properties, in particular on the effective crack velocity exponent? At the more fundamental level, what are the underlying physical processes responsible for the R-curve, and how do these processes relate to the material microstructure? The future success in developing ultra-strength ceramics surely rests with the answers to questions like these.

In this paper we survey the results of recent studies in these laboratories[2-5] aimed at elucidating the nature of R-curve behavior in selected aluminas and glass-ceramics, materials in which the elements of the microstructure are reasonably well understood. In our experiments indentation flaws are introduced into strength bars, so that the size of the crack which leads to failure may be varied systematically. This conveniently allows us to bridge the gap in scale of fracture from the traditional macroscopic test specimen down to the microstructurally-determined flaw. Moreover, the origin of failure is now predetermined, so we can follow the crack evolution directly during an actual strength test. As we shall see, these experiments provide new insights into the fracture mechanisms. A stress intensity factor for the microstructural influence on the net crack driving force is thereby determined, at two levels of rigor: first, semi-empirically (i.e. without recourse to a specific R-curve mechanism), sufficient to account for the trends in both inert and dynamic-fatigue strength data; second, in terms of a specific physical model of distributed restraining forces behind the crack front. The restraining forces in the latter instance are associated with the formation of microstructurally-localized ligaments across the separating fracture interface.

2. EXPERIMENTAL

We have conducted a test program on several ceramics.[2,3] Here we present results on three representative aluminas - single crystal sapphire, polycrystal nominally "pure" (Coors Vistal), polycrystal with 1% grain boundary glassy phase (Freidrichsfeld F99) - and two glass-ceramics - low expansion (Corning C9606, Pyroceram) and machinable (Corning C9658, Macor). Specimens were prepared in disk or bar form suitable for strength testing.

Most of the specimens were indented with a Vickers diamond at the centers of the prospective tensile faces. Some specimens were left unindented as controls. The range of contact loads covered was 1 to 300 N. The strengths of the specimens were determined in biaxial or four-point flexure. These flexure tests were run in either inert environment (silicone oil), to determine the toughness characteristics,[2] or fatigue environment (water), to determine crack velocity characteristics.[3]

Optical microscopy was used to examine the fracture patterns, both after and during the testing to failure. The post-indentation

examination was needed to confirm the indentation flaw as the source of failure. It also provided useful information on the crack morphology. However, the most revealing observations were those made in situ, as the flexural loading was being applied. For this latter purpose, a special loading facility was attached directly to the stage of an inverted microscope, with the indented specimen surface facing downward, allowing the entire crack evolution to failure to be monitored. A video recording attachment was extremely beneficial in helping to interpret some of the seemingly complex features of the crack growth behavior enroute to failure.

3. INTERPRETATION AND DISCUSSION OF RESULTS

3.1 Inert Strengths and R-Curves

Inert strength data are shown as a function of indentation load, $\sigma_m(P)$, for the aluminas and glass-ceramics in Figs. 1(a,b,c) and 2(a,b), respectively. Individual data points represent means and standard deviations (evaluated in logarithmic coordinates) for breaks at indentation flaws at each prescribed load. Hatched regions at left of each plot represent strengths of the unindented controls. The solid curves are theoretical fits to the data (see below).

It is immediately apparent, even without a detailed fracture mechanics analysis, that there is disparate behavior in the strength responses within each material class. This is seen most clearly in the alumina data of Fig. 1. The sapphire data plot more or less in accordance with the simple power-law relation $\sigma_m \propto P^{-1/3}$ from "ideal" indentation theory[6,7] (i.e. with microstructure terms excluded). Insofar as the proportionality factor in this relation involves the material

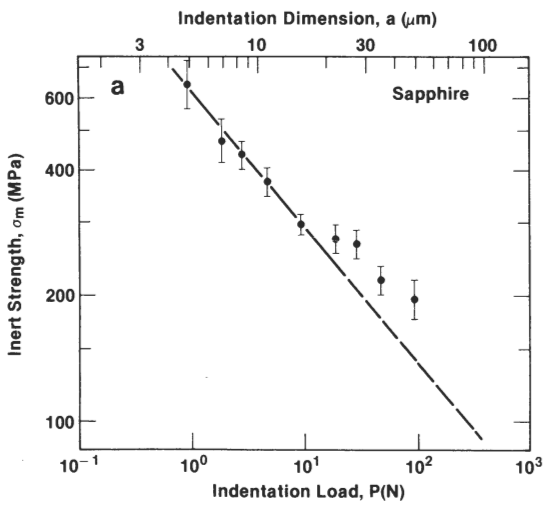

Figure 1. Inert strength as function of indentation load for three aluminas. Upper horizontal axis shows equivalent flaw size, plotted as indentation half-diagonal. After Ref. 2.
(b and c continued on next page)

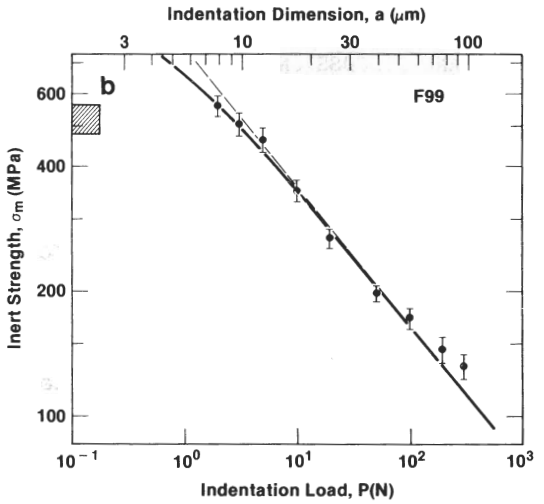

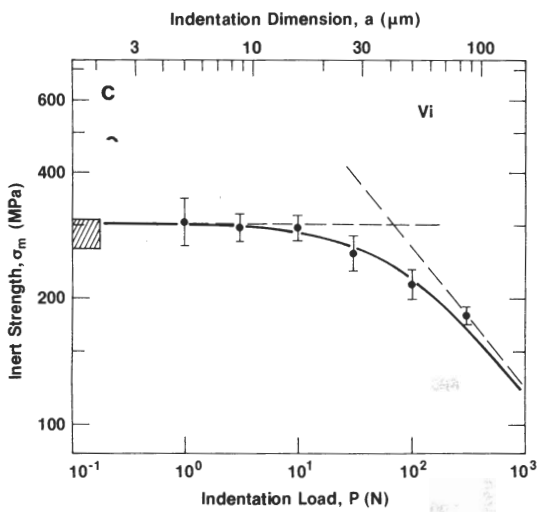

Figure 1. (Continued)

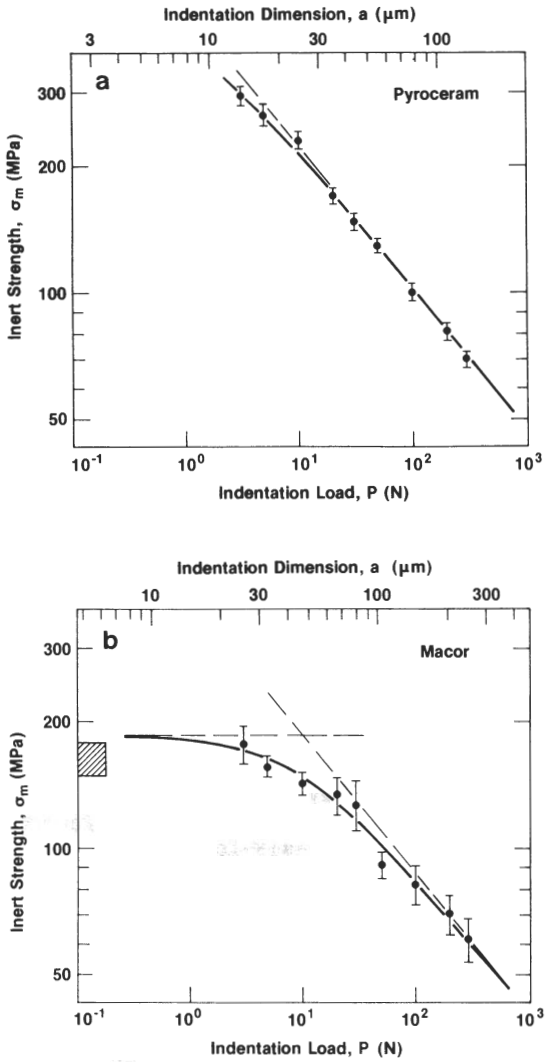

Figure 2. Inert strength as function of indentation load for two glass-ceramics.

toughness (see Eq. 3 below), we may regard the linear fit in this case as an extrapolation from large-scale crack resistance data. The data for the polycrystalline aluminas show indications of a low-load "saturation" in strength levels, much more so in the Vi than in the F99 material. In these cases the extrapolations from macroscopic toughness evaluations, represented as the inclined broken line asymptotes, overestimate the strengths in the small-flaw region. The need to include a microstructural term into the strength analysis is evident.

The starting point for such an analysis is an appropriate stress intensity factor.[2] For an indentation crack of size c, formed at contact load P and subsequently subjected to a bending stress σ_a, we may write

$$K = K_a + K_r + K_m$$

$$= \psi\sigma_a c^{1/2} + \chi P/c^{3/2} + K_m(c,d,.....) = T \qquad (1)$$

where the equality with intrinsic toughness T (referred to elsewhere as K_c) denotes a state of equilibrium (pertinent to inert testing conditions). Here ψ is a crack geometry constant ($\cong 2/\pi^{1/2}$), χ is a residual contact field parameter, and d is some characteristic dimension of the crack-microstructure interaction. The object of the exercise is to determine K_m (c,d,....) explicitly for given microstructural systems. Then we may solve Eq. 1 for the critical stress σ_m at failure (i.e. the inert strength) by imposing the instability requirement dK/dc = 0.

In the absence of any knowledge as to the specific mechanism of crack-microstructure interaction we can only proceed by semi-empirical representation of K_m. This was effectively the approach adopted in Ref. 2 (see also Ref. 8). In terms of the current terminology, we may write the microstructural functional from that earlier work in the form, for $c \geq d$,

$$K_m = -(\mu Q/d^{3/2})[1 - (d/c)^{3/2}] \qquad (2)$$

where Q is some microstructurally associated "force" (real or effective) and μ is a constant. We note that $K_m = 0$ at c = d, designating a cutoff crack size below which the toughness is determined exclusively by the intrinsic value T. At $c > d$, K_m becomes increasingly negative so that the toughness, insofar as it may be considered to be augmented by this term (i.e. $T-K_m$ in Eq., 1), appears as a rising function of crack size. It is Eq. 2 which provides the basis for the curve fits in Figs. 1 and 2.

Once we have an explicit expression for Eq. 1, we should be able to invert the solution to determine the effective R-curve (or perhaps more strictly, in our present notation, T^*-curve) characteristics from the $\sigma_m(P)$ data. Indeed, we can carry out such an inversion for individual data points without a full solution, by calculating an "apparent" toughness from a base formula representative of the microstructure-free state (i.e. with $K_m = 0$ in Eq. 1). Thus we can show that

$$T^* = \eta(\sigma_m P^{1/3})^{3/4} \qquad (3)$$

where $\eta = \eta(\psi,\chi) = 0.88$ is determined by experimental calibration,[9] and where the asterisk is to signify that we intend to use Eq. 3 outside the strict realms of its applicability (which is along the linear asymptotes of slope -1/3 in Figs. 1 and 2). In this way, we plot the apparent toughness vs load data for the aluminas and glass-ceramics in Figs. 3 and 4, respectively. The R-curve tendencies are clearly illustrated in these plots. Particularly noteworthy is the way in which the data for Vi alumina in Fig. 3 cross those for the other two aluminas, indicating

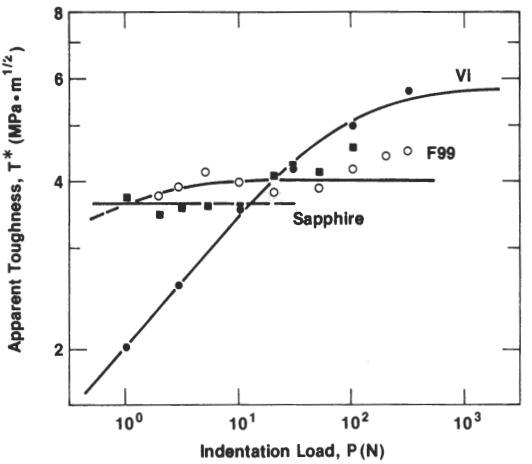

Figure 3. Apparent toughness (evaluated from Eq. 3) as function of indentation load for the aluminas represented in Fig. 1. Note tendency for polycrystal data (especially Vi) to cross above the sapphire data at high loads.

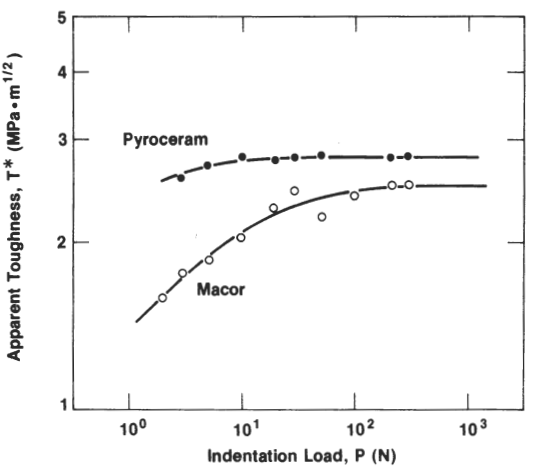

Figure 4. Apparent toughness as function of indentation load for the glass-ceramics represented in Fig. 2.

that toughness evaluations made in the macroscopic region can be totally misleading in assessing the relative merits of different materials at the microstructural flaw level. The solid curves in these plots are again fits using the empirical function Eq. 2 to obtain analytical solutions to $T^*(P)$ from Eq. 1.[2]

3.2 Fatigue Strengths and Crack Velocity Exponents

Figures 5 and 6 show dynamic fatigue strength as a function of stressing rate, $\sigma_f(\dot{\sigma}_a)$, for those materials which displayed the strongest R-curve behavior in the preceding subsection, viz. Vi alumina and Macor glass-ceramic. The results are obtained for two indentation loads, towards opposite ends of the R-curves, for each material. Data points represent means and standard deviations (log coordinates) at each stressing rate. Horizontal broken lines at right are inert strength limits at the appropriate loads. The solid lines are linear fits in accordance with theoretical prediction (below), notwithstanding some apparent curvature in the plots.

We see that, despite the extreme R-curve behavior shown by these two materials, there is no significant sensitivity of the fatigue susceptibility to crack size; the curves for different values of P in Figs. 5 and 6 are closely parallel.

An analytical basis for explaining this insensitivity can be established by combining the stress intensity factor K(c) in Eq. 1 (in the subcritical region $K < T$) with a crack velocity function $v(K)$,[3] here assumed to be of standard power-law form[#]

$$v = AK^n. \tag{4}$$

The resultant formulation is a differential equation which, for constant $\dot{\sigma}_a$ and empirical K_m function in Eq. 2, has a solution of the same form as that for Griffith-like flaws,

$$\sigma_f = (\lambda' \dot{\sigma}_a)^{1/(n'+1)} , \tag{5}$$

differing only in the values of the exponent and intercept terms (hence the prime notation). It turns out that the exponent n' is related to the true crack velocity exponent n via the simple transformation equation

$$n' = 3n/4 + 1/2 \tag{6}$$

totally independently of P. This accounts for the parallelism between the curves in Figs. 5 and 6. The intercept λ' does turn out to be dependent on P, however, and this needs to be allowed for in any complete description of fatigue properties.[3]

3.3 Direct Observations of Crack Growth in Strength Specimens

Observations of the crack response to the applied loading provide valuable clues to the mechanism responsible for the rising R-curve behavior described earlier.[4] We have looked at all the materials represented in the strength data plots, but have focussed particularly on the Vi alumina, the material with the strongest effect. Optimal conditions for microscopy were obtained by polishing the surfaces down to

---

[#]There are several subtleties in writing the crack velocity function this way for materials with rising R-curves. These subtleties will be explored elsewhere.

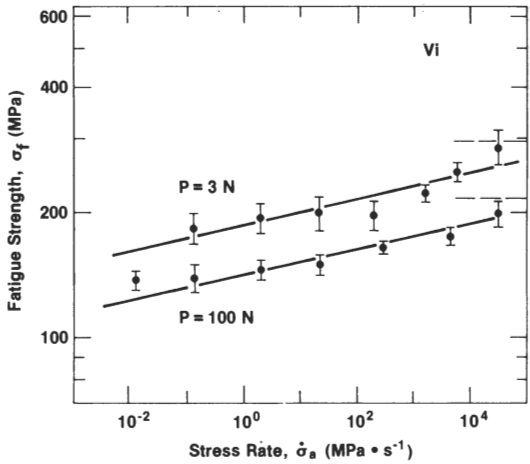

Figure 5. Dynamic fatigue plots for Vi alumina at two indentation loads. After Ref. 3.

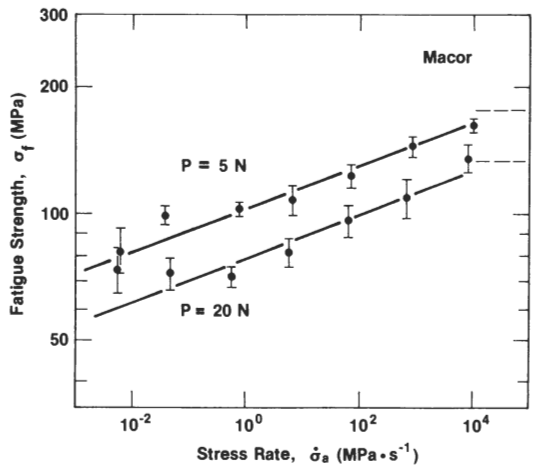

Figure 6. Dynamic fatigue plots for Macor glass-ceramic at two indentation loads.

0.3 μm Al_2O_3 paste, thermally etching to reveal the grain boundaries, and metal coating to improve the reflectivity.

The first microscopy examinations made were of the final failure patterns. Some of the general features of these patterns are evident in Fig. 7, which shows the immediate region around the indentation in a fractured Vi alumina disk. It is seen that the fracture is almost exclusively intergranular, once the initial radial cracks traverse the first grains containing the indentation impression. This intergranular mode was evident in all the aluminas we tested, regardless of degree of R-curve behavior. This is not unexpected, of course, in view of the distinct tendency for the $T^*(P)$ polycrystal data to cross below the single crystal data at low P in fig. 3. An analogous "intergranular" mode was observed in the glass-ceramics, with matrix cracks propagating around rather than straight through the larger second-phase crystallites.[10,11] In all cases well-defined primary cracks were observed, with no obvious subsidiary bifurcation or microcracking.

Post-test inspections in Vi revealed one further, telling piece of information. At failure (marked by an abrupt drop in applied stress to zero) the radial cracks propagated to the edges of the specimens. Continuous traces of these cracks could be followed along both top and bottom surfaces. Yet the specimens did not fragment - some additional applied force was necessary to separate the pieces. It appeared that there must be remnant links of some kind across the "broken" interfaces.

It was in this connection that the in situ observations were most revealing, especially on the Vi alumina. Tests were run at slow stressing rates, in air, to allow each step in the crack growth sequence to be followed carefully. In the initial stage of loading the cracks remained quite stationary. Then one arm of the radial crack pattern extended abruptly, typically over 5 to 10 grain diameters. Further loading produced more such jumps, either in the same or adjacent arms, with increasing frequency, until failure occurred. Similar initiations were occasionally observed from prominent "natural" flaws.[12] The picture we conjure up is one of highly stable, but erratic, growth prior to failure.

The stable growth comes as no surprise, since it is well established that the residual stress term K_r in Eq. 1 (by virtue of its inverse dependence on crack size) manifests itself in precisely this way.[6] But what causes the discrete jump-arrest sequences? Closer inspection of the separating crack behind the main advancing front provides important clues. There are points where the crack appears to be disjointed on the microscale, as though the main front has had some difficulty in deciding which way it might propagate around a certain grain (or second-phase particle). An extreme example is shown in Fig. 8. Rarely did the distance between the adjacent crack segments exceed more than one or two grain diameters (including in the subsurface direction, as indicated by interrupting the test and viewing in transmitted light). Independent observations of such regions by Swanson in these laboratories[13] have demonstrated the continued evolution of the crack segments at distances greater than 1 mm behind the main front in Vi alumina. This evolution ceases only when one of these segments runs back into the plane of the other, at which point the opposing crack walls completely separate. In "favorable" cases the two segments link up simultaneously, causing grain "pop-outs" (e.g. in upper left of crack trace, Fig. 7).

We are led to conclude that the crack is "hung up" by grain-localized, restraining ligaments distributed over the separating crack interface. This conclusion is consistent with the "memory effect"

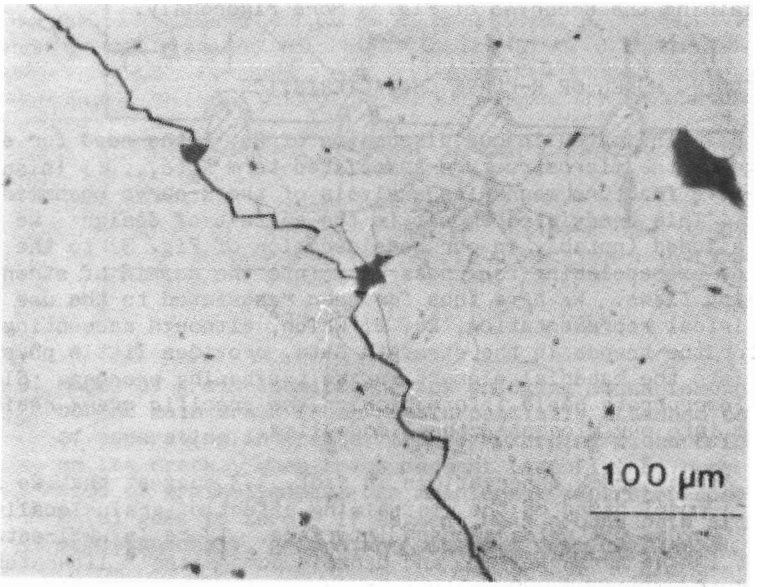

Figure 7. Optical micrograph of Vickers indentation site in a fractured Vi alumina disk. Note well-defined primary, intergranular crack patterns.

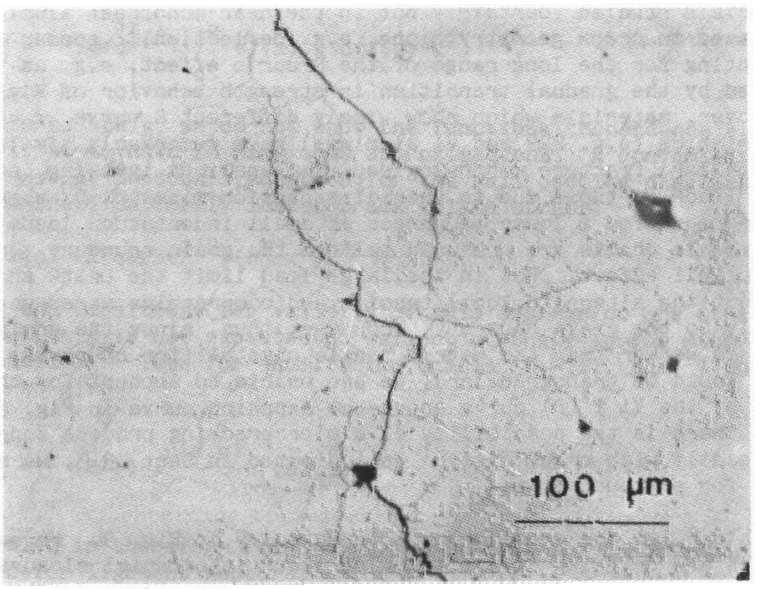

Figure 8. Micrograph showing apparently disjointed crack segments along main fracture path in Vi alumina.

reported by Knehans and Steinbrech;[14] that any previous progression up an R-curve can be negated by cutting away material from the walls of the extended crack (e.g. by sawcutting). We now have an experimental basis for explaining the R-curves of Fig. 3 more rigorously.

4. BRIDGING MODEL OF R-CURVE CHARACTERISTICS

We have indicated in our discussion of Eq. 1 the need for explicit knowledge of the microstructure-associated term $K_m(c,....)$ in any quantitative fracture mechanics analysis of the R-curve phenomenon in ceramics. This need is paramount in the context of design: we have already alluded (notably in our consideration of Fig. 3) to the potential dangers of extrapolating toughness data into the domain of strength-controlling flaws. We have thus far been restricted to the use of a semi-empirical representation, Eq. 2, which, although accounting well enough for the trends in the strength data, provides little physical insight into the material element in the toughening process. Clearly, we have to incorporate basic information on the specific crack resistance mechanism into our microstructural modelling.

The direct crack observations in Sect. 3.3 suggest that we should consider a model based on the restraining effect of grain-localized "bridges" across the primary crack interface. There is well-established precedent in the concrete[15-17] and ceramic composites[18] literature for this kind of modelling. Our aim in this section is to outline how one sets up the fracture mechanics, leaving the details of the calculations to a separate paper.[5]

Before proceeding with our bridging model, however, it is well that we should give reasons for discounting other mechanisms which have been proposed to account for apparent toughening effects.[1] The most vaunted of the R-curve mechanisms, transformation toughening, does not operate in the materials studied (certainly not in the near-monophase aluminas). Models based on crack geometry alone, e.g. deflection,[19] appear incapable of accounting for the long range of the R-curve effect, e.g. as manifested by the gradual transition in strength behavior of Figs. 1 and 2. Moreover, materials which show widely different R-curve characteristics (e.g. F99 and Vi aluminas) have remarkably similar (intergranular) fracture morphologies. Explanations invoking internal stresses (such as those due to thermal expansion mismatch)[20] appear to be able to account for a lower toughness at small indentation loads, where the microscale cracks are presumed to feel the grain boundary tensile forces to full effect. But in the large-load limit the crack should average out the alternate local tensile and compressive stresses, tending ultimately to the grain boundary toughness; thus, since the grain boundary is weaker than the matrix single crystal (for otherwise the fracture would be transgranular), we are unable to account for the crossing of the Vi $T^*(P)$ curve above the sapphire curve in Fig. 3. Finally, there is the possibility of a microcracking process zone which grows steadily with crack size;[21] as indicated in Sect. 3.3, we saw no evidence for any such zone.

Consider now the model shown schematically in Fig. 9. We suppose that there are bridging ligaments which exert interfacial closure forces $F_i(x,z)$ behind the advancing crack tip. It is assumed, as in the case of fiber-reinforced ceramic composites,[18] that these forces can be considered to be continuously distributed, $F_i(x,z) = \sigma_i(x)\, d^2$, once the crack extends beyond the first bridges, where d is the mean spacing between bridging sites. This assumption represents a compromise between retention of an element of discreteness and mathematical tractability.

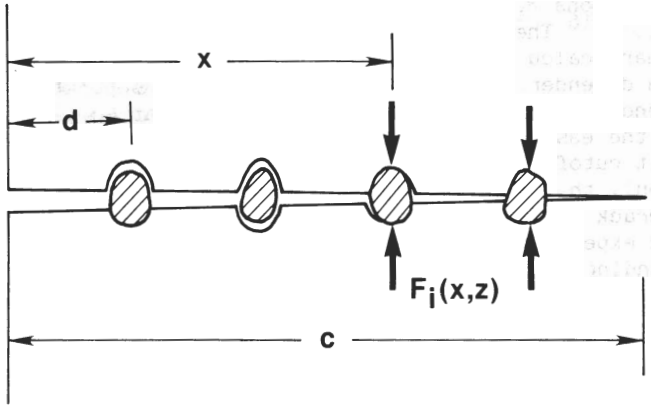

Figure 9. Model of grain-localized crack bridging mechanism. Grains behind main crack front remain partially attached to both sides of separating interface, thereby exerting closure forces $F_i(u)$ on the crack. When crack segment (see Fig. 8) runs around one side of grain ligament the main crack separates completely, $F_i(u)$ goes to zero. If segment runs around both sides simultaneously, grains are detached from surface.

Then we may resort to standard Greens function solutions for the stress intensity factor.[22] In the case of penny-like cracks pertinent to the indentation geometry we have (treating closure forces as positive here)

$$K_m = - (\psi/c^{1/2}) \int_d^c \sigma_i(x)\, x\, dx/(c^2-x^2)^{1/2}. \qquad (7)$$

Unfortunately, we do not know the functional dependence $\sigma_i(x)$ a priori, so we have to make some approximations. A convenient ploy is to make use of Sneddon's equation for the wall opening displacements of a traction-free, uniformly loaded crack (plane stress)[23]

$$u(x,c) = (\psi K/Ec^{1/2})(c^2-x^2)^{1/2} . \qquad (8)$$

None of the conditions for validity of this expression are strictly met here, but this is not expected to reflect strongly in the material dependencies.[18] Then for equilibrium cracks (K = T), Eqs. 7 and 8 combine to give

$$K_m = - (E/T) \int_o^{u(d,c)} \sigma_i(u)\, du . \qquad (9)$$

The problem is therefore reduced to determining the force-separation function for ligament rupture, which of course is dependent on the details of the rupture process.

Once $\sigma_i(u)$ has been determined, the requisite stress intensity factor $K_m(c,d,....)$ may be evaluated. We note that the crack-size dependence enters via the upper limit in Eq. 9 (in conjunction with Eq. 8). To this point our evaluations of Eq. 9 have been restricted to

trial functions $\sigma_i(u)$, of the kind proposed in the analysis of concrete fracture.[15,16] There are some encouraging trends emerging from our preliminary calculations, however. Thus we find that the $K_m(c)$ function, although dependent on the choice of the force-separation curve, is in all cases monotonically increasing (indicating that Eq. 2 does at least contain the essence of the crack-size influence). Also, by virtue of the low limit cutoff in Eq. 7 (below which the toughening mechanism is not in operation), the calculations lead to the prediction of the same kind of radial crack pop-in behavior as observed in the indentation-strength experiments earlier (Sect. 3.3). On the other hand, a full understanding of the role of material properties, apart from E and T in Eq. 9, awaits further development of the micromechanics of ligament rupture (via $\sigma_i(u)$). Only then can we expect to account for such factors as grain boundary phase (as is so clearly manifest in the contrasting R-curves for Vi and F99 aluminas in Fig. 3, Sect. 3.1), grain size, etc.

5. CONCLUSIONS

(i) Indentation-strength techniques provide a powerful methodology for analyzing the dependence of toughness and fatigue properties of brittle ceramics on crack size.

(ii) Microstructural influences are strongly felt in the inert strength data, reflecting R-curve behavior. They have relatively no effect on the slopes of the dynamic fatigue plots (at least in the crack-size range covered here).

(iii) The experimental R-curves depend sensitively on the microstructural detail, e.g. grain boundary phase.

(iv) Direct observations of the crack evolution to failure suggest that "toughening" in the aluminas and glass-ceramics is due to the closure effect of unruptured grain-scale ligaments behind the main crack front. The basis of a fracture mechanics description of this process is outlined.

ACKNOWLEDGEMENTS

The authors wish to thank P.L. Swanson and B.J. Hockey for many useful discussions on parts of this work, particularly in relation to the observations in Sect. 3.3. Funding was provided by the U.S. Air Force Office of Scientific Research.

REFERENCES

1. S. M. Wiederhorn, Ann. Rev. Mater. Sci. 14; 373 (1984).
2. R. F. Cook, B. R. Lawn and C. J. Fairbanks, J. Amer. Ceram. Soc., in press.
3. R. F. Cook, B. R. Lawn and C. J. Fairbanks, J. Amer. Ceram. Soc., in press.
4. P. L. Swanson, C. J. Fairbanks, B. J. Hockey, B. R. Lawn and Y. W. Mai, in preparation.
5. Y. W. Mai and B. R. Lawn, in preparation.
6. D. B. Marshall, B. R. Lawn and P. Chantikul, J. Mater. Sci. 14; 2225 (1979).
7. B. R. Lawn, p. 1 in Fracture Mechanics of Ceramics, Vol. 5, R. C. Bradt, A. G. Evans, D. P. H. Hasselman and F. F. Lange, eds., Plenum, New York (1983).

8. A. G. Evans, J. Am. Ceram. Soc. 63; 115 (1980).
9. P. Chantikul, G. R. Anstis, B. R. Lawn and D. B. Marshall, J. Am. Ceram. Soc. 64; 539 (1981).
10. R. Morena, K. Niihara and D. P. H. Hasselman, p. 145 in Fracture Mechanics of Ceramics, Vol. 5, R. C. Bradt, A. G. Evans, D. P. H. Hasselman and F. F. Lange, eds., Plenum, New York (1983).
11. R. Morena, K. Niihara and D. P. H. Hasselman, J. Am. Ceram. Soc. 66; 673 (1983).
12. T. Okada, G. Sines and D. J. Green, J. Am. Ceram. Soc. 65; C-64 (1982).
13. P. L. Swanson, private communication.
14. R. Knehans and R. Steinbrech, J. Mater. Sci. Letters 1; 327 (1982).
15. A Hillerborg, M. Modeer and P. E. Petersson, Cement and Concrete Res. 6; 773 (1976).
16. M. Wecharatana and S. P. Shah, J. Eng. Mechs. Div., ASCE 109; 1231 (1983).
17. Y. W. Mai, in Application of Fracture Mechanics to Cementitious Composites, S. P. Shah, ed., Martinus Nijthoff, Netherlands, in press.
18. D. B. Marshall, B. N. Cox and A. G. Evans, in preparation.
19. K. T. Faber and A. G. Evans, Acta Met. 31; 565, 577 (1983).
20. R. W. Rice, R. C. Pohanka and W.J. McDonough, J. Am. Ceram. Soc. 63; 703 (1980).
21. A. G. Evans and K. T. Faber, J. Am. Ceram. Soc. 67; 255 (1984).
22. G.C. Sih, "Handbook of Stress Intensity Factors," Lehigh University, Bethlehem (1973).
23. I. N. Sneddon and M. Lowengrubb, "Crack Problems in the Classical Theory of Elasticity," Wiley, New York (1969).